The complex structure of liquid Cu_6Sn_5 alloy

2009 J. Phys.: Condens. Matter 21 155106

(http://iopscience.iop.org/0953-8984/21/15/155106)

J. Phys.: Condens. Matter **21** (2009) 155106 (7pp) doi:10.1088/0953-8984/21/15/155106

The complex structure of liquid Cu_6Sn_5 alloy

Jingyu Qin[1], Hui Liu[2], Tingkun Gu[1] and Xiufang Bian[1]

[1] The Key Laboratory of Liquid Structure and Heredity of Materials, Ministry of Education, Shandong University, Southern Campus, Jinan 250061, People's Republic of China
[2] Shandong High Performance Computing Center, Shandong University, Southern Campus, Jinan 250061, People's Republic of China

Received 11 December 2008, in final form 4 March 2009
Published 20 March 2009
Online at stacks.iop.org/JPhysCM/21/155106

Abstract

By applying *ab initio* molecular dynamics simulation to liquid Cu_6Sn_5 alloy, the hetero-coordination tendency is discovered by Bathia–Thornton partial correlation functions and a chemical short-range parameter. However the local structural environment of Sn in l-Cu_6Sn_5 alloy resembles that of liquid Sn by Voronoi analysis. A new feature, i.e. a subpeak in between the first and second peaks, is discovered by the present method which implies that topologically disordered β-Sn-type structural units may exist in l-Cu_6Sn_5 alloy. The local density states of electrons show that both Cu–Sn and Sn–Sn bonding exist in l-Cu_6Sn_5 alloy. This work suggests that chemical short-range order between unlike atoms and self-coordination between Sn atoms coexists in l-Cu_6Sn_5 alloy.

(Some figures in this article are in colour only in the electronic version)

1. Introduction

In 1966, Enderby *et al* [1] determined the partial structural functions of liquid Cu_6Sn_5 alloy by using the technique of neutron diffraction with isotopic substitution. Then in 1970, North *et al* [2] performed x-ray scattering experiments to get the partial structural functions of l-Cu_6Sn_5 alloy by assuming that the partial structural functions are independent of atomic concentration. The x-ray absorption fine structure (XAFS) technique was also applied to the investigation of the local structure of l-Cu_6Sn_5 alloy [3], by which it is found that the shape of the $g_{CuCu}(r)$ and $g_{SnSn}(r)$ is affected by the presence of unlike atoms and therefore the assumption of the independence of atomic concentrations as the basis of previous XRD studies [2] is not fully justified. However, XAFS experiments are not sensitive to the structure beyond the first coordination shell.

Recently, the structure of l-Cu_6Sn_5 alloy was again studied by Kaban *et al* [4] through applying reverse Monte Carlo (RMC) simulation on the data from x-ray and neutron diffraction. On the one hand, a slight tendency to self-coordination was suggested based on partial coordination number analysis. However, on the other hand, by applying the micro-inhomogeneous model, a Cu_3Sn-type cluster is suggested to be one of the basic alloys existing in l-Cu_6Sn_5 alloy. Cu_3Sn is an intermetallic compound which has a much higher melting temperature than the intermetallic compound η'-Cu_6Sn_5 [5]. This means that micro-heterogeneous clusters exist in l-Cu_6Sn_5 alloy. These two avenues are seemingly in conflict with each other.

In η'-Cu_6Sn_5, from 0.263 to 0.286 nm, an Sn atom may have Cu atoms with as many as 20 kinds of Sn–Cu distances, while Sn atoms have the shortest Sn–Sn distance of about 0.331 nm. From 0.254–0.272 nm a Cu atom may have other Cu atoms with as many as 6 kinds of Cu–Cu distances. The shortest Sn–Cu distance (0.263 nm) is much less than the average of the shortest distances of Cu–Cu (0.254 nm) and Sn–Sn (0.331 nm). This means that there exists a strong affinity between some Sn and Cu atoms. Though the crystalline structure is very complex, especially in the case of the Sn local environment, some Sn atoms are preferentially coordinated by Cu atoms.

After melting, such a characteristic may persist into the liquid state. Furthermore, in research works [1–4] on l-Cu_6Sn_5 alloy the atomic distance between unlike atoms is obviously shorter than the mean of the two like-atom distances. This phenomenon also implies that the affinity between unlike atoms is rather strong and seems to be incompatible with the self-coordination preference found in [4].

By checking the existing experimental results we find that the structure of liquid Cu_6Sn_5 alloy may be more complex

than expected and needs to be investigated further by other methods. *Ab initio* molecular dynamics (AIMD) simulations have been widely employed to investigate the structure of different kinds of liquid alloys. For example, though there were experimental partial pair correlation functions (PCFs) of liquid $Al_{80}Ni_{20}$ alloy, recently the application of AIMD simulation on such an alloy provided a clear picture of the icosahedron's clusters [6]. Apart from the published experimental results on l-Cu_6Sn_5 alloy by different techniques, the application of AIMD simulation is then expected to supply detailed local structure information alternatively.

This paper was arranged as follows. Section 2 describes the details of our AIMD simulations, in section 3 we firstly compare the calculated pair correlation functions of liquid Cu and Sn with the experimental results, and then present our structural analysis on l-Cu_6Sn_5 alloy. Section 4 shows the local structural character by Voronoi analysis on l-Cu_6Sn_5 alloy. Section 5 is about the electronic structure of liquid Cu_6Sn_5 alloy. The dynamical properties of l-Cu_6Sn_5 alloy are included in section 6. Section 7 is a summary.

2. AIMD details

The AIMD simulations were carried out using the most recent version of the Vienna *ab initio* simulation package (VASP) [7] in which the interactions between the ions and electrons are described by the projector augmented-wave method [8]. Simulations were performed using a gradient-corrected energy functional [9]. The plane-wave basis set contained components with energies up to about 273 eV. A cubic cell containing 77 atoms with periodic boundary condition was used to simulate the liquid system. We employed the density 48.8 nm^{-3}, 34.3 nm^{-3} and 74.9 nm^{-3} for liquid Cu_6Sn_5 alloy, liquid Sn and Cu, respectively. For liquid Cu_6Sn_5 alloy, the pressure of the system is about −8.6 kBar at 913 K. Only the Γ-point was used to sample the supercell Brillouin zone.

All the dynamical simulations were carried out in the canonical ensemble (NVT) through a Nosé [10] thermostat with a characteristic frequency equal to 52 ps^{-1}. Newton's equations of motion were integrated using the Verlet algorithm with a time step of 3 fs. For liquid Cu, Sn and Cu_6Sn_5 alloy, the systems were simulated at $T = 1473$ K, 873 K and 913 K for 9 ps, respectively. The partial PCFs are evaluated by equation (1) from the configurations which span the last 6 ps:

$$g_{\alpha\beta}(r) = c_\beta^{-1}\rho_0^{-1}N_\alpha^{-1}\left\langle\sum_{\mu=1}^{N_\alpha}\sum_{\gamma=1}^{N_\beta}\delta\{r-(r_{\alpha\mu}-r_{\beta\gamma})\}\right\rangle. \quad (1)$$

The partial structure factors are updated according to equation (2), and then the total structure factor of Faber–Ziman type is calculated through equation (3):

$$S_{\alpha\beta}(Q) = (N_\alpha N_\beta)^{-1}\left\langle\sum_{\mu=1}^{N_\alpha}\sum_{\gamma=1}^{N_\beta}e^{iQ\cdot(r_{\alpha\mu}-r_{\beta\gamma})}\right\rangle \quad (2)$$

$$S_{\text{total}}(Q) = \sum_\alpha\sum_\beta\frac{c_\alpha c_\beta f_\alpha(Q)f_\beta(Q)}{(c_\alpha f_\alpha(Q)+c_\beta f_\beta(Q))^2}S_{\alpha\beta}(Q). \quad (3)$$

Table 1. First peak positions of $g_{\alpha\beta}(r)$ by different methods.

Methods	r_{CuCu} (nm)	r_{CuSn} (nm)	r_{SnSn} (nm)
AIMD	0.253	0.270	0.326
X-ray [2]	0.260	0.269	0.315
XAFS [3]	0.253	0.267	0.307
RMC [4]	0.26	0.26	0.32

In equations (1)–(3) c_β and N_α are the concentration and atomic number of the βth and αth elements in the alloy, respectively. ρ_0 is the averaged number density of the liquid Cu_6Sn_5 alloy. $r_{\alpha\mu}$ is the position vector of the μth atom of the αth element. $f_\alpha(Q)$ is the x-ray scattering factor of the αth element. The brackets $\langle\cdots\rangle$ here denote the time average. The partial coordination numbers are evaluated by equation (4):

$$N_{\alpha\beta} = \int_0^{r_{\min}} 4\pi r^2 c_\beta\rho_0 g_{\alpha\beta}(r)\,dr \quad (4)$$

where $N_{\alpha\beta}$ means that there are $N_{\alpha\beta}$ atoms of the βth element around an atom of the αth element on average. $r_{\min}$ is the location of the minimum in between the first and second peaks in $g_{\alpha\beta}(r)$. The Bathia–Thornton (BT) partial PCFs are then evaluated through equations (5)–(7) [11]:

$$g_{NN}(r) = c_{Cu}^2 g_{CuCu}(r) + c_{Sn}^2 g_{SnSn}(r) + 2c_{Cu}c_{Sn}g_{CuSn}(r) \quad (5)$$

$$g_{CC}(r) = c_{Cu}c_{Sn}[g_{CuCu}(r) + g_{SnSn}(r) - 2g_{CuSn}(r)] \quad (6)$$

$$g_{NC}(r) = c_{Cu}[g_{CuCu}(r)-g_{CuSn}(r)]+c_{Sn}[g_{SnSn}(r)-g_{CuSn}(r)]. \quad (7)$$

3. Structural functions of l-Cu, l-Sn and l-Cu_6Sn_5 alloy

To verify the reliability of the AIMD simulation on l-Cu_6Sn_5 alloy, we first performed AIMD simulations on both l-Sn and l-Cu. In fact, Cu and Sn have rather different liquid structures. The structure of l-Cu can be simply modeled by hard sphere packing [12], while l-Sn has a rather complex structure with a shoulder at the right of the first peak in the structure factor [13].

The calculated PCFs of both l-Sn and l-Cu are shown in figure 1 with the corresponding experimental curves [12, 13] for comparison. In general, the calculated $g(r)$'s of both l-Sn and l-Cu fit well with the experimental ones. For l-Sn, the first peak position of the experimental curve at 0.312 nm is well reproduced by AIMD simulation at 0.310 nm, while, for l-Cu, the first peak of $g(r)$ at 0.247 nm agrees well with the peak in the experimental curve at 0.250 nm. This indicates that the AIMD simulations can be applied in Cu–Sn alloys.

The static structure factors of l-Cu_6Sn_5 alloy are shown in figure 2. The first peak of $S_{SnSn}(Q)$ is more diffused than that of $S_{CuCu}(Q)$ and $S_{CuSn}(Q)$. The total structure factor by AIMD is in good agreement with the experimental curve [4].

Then, we depict the calculated $g_{\alpha\beta}(r)$ (α, β = Sn, Cu) with those by experiments in figure 3 and the first peak positions of these curves are compiled in table 1.

Firstly, it is helpful to compare these parameters given by AIMD simulation with those of the crystalline phase. We

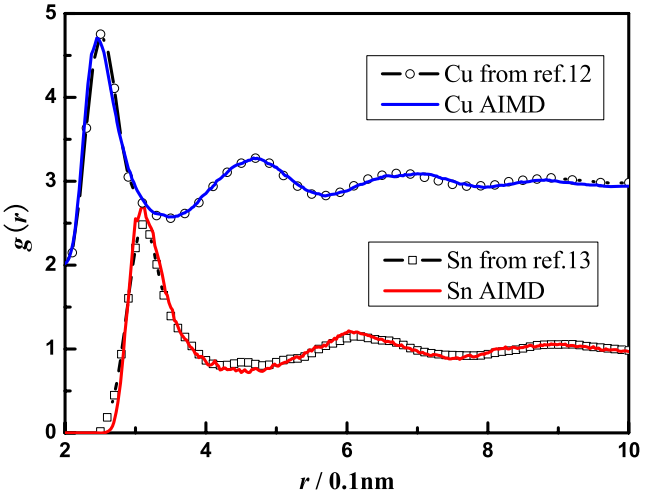

Figure 1. PCFs of both *l*-Sn and *l*-Cu by AIMD simulations and experiments [12, 13].

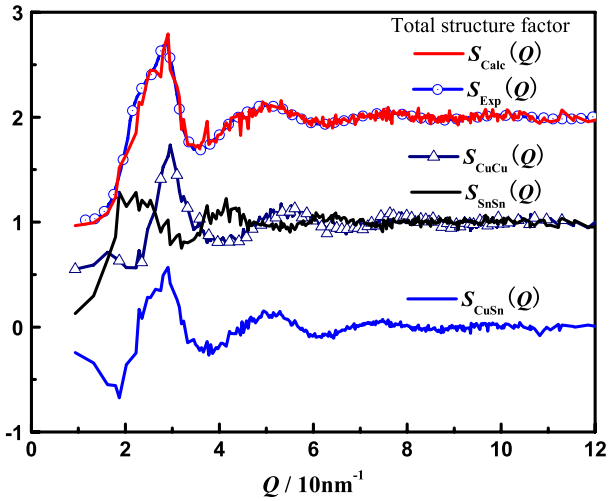

Figure 2. The static structure factors of liquid Cu_6Sn_5 alloy by AIMD simulation.

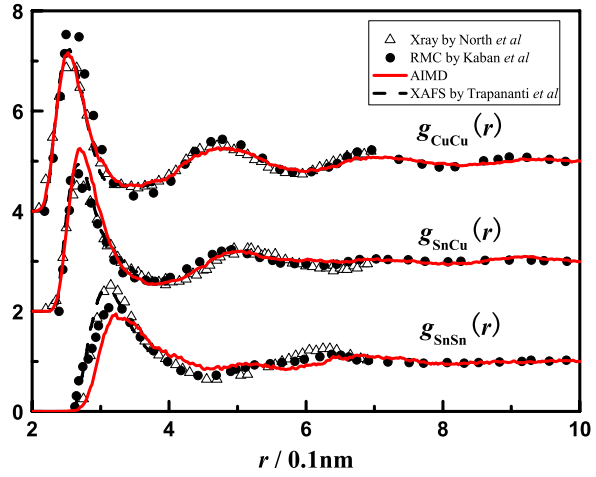

Figure 3. Comparison of PCFs of *l*-Cu_6Sn_5 alloy by different methods (curves except for AIMD simulation are digitized from [2–4]).

can show that the coordination shells separated by nearest distances in the crystalline phase should merge into a diffused coordination shell in the liquid state. The nearest Cu–Cu distance in the crystalline state is 0.254 nm, very close to the value 0.253 nm in the liquid state. For the Sn–Cu distance its mean value in the crystalline state is 0.274 nm, while in the liquid state it is 0.270 nm. The Sn–Sn distance in the liquid state is 0.326 nm, which is comparable with the shortest Sn–Sn distance of 0.331 nm in the intermetallic compound.

From table 1, we find that r_{CuSn} equals r_{CuCu} is a remarkable feature of the results by RMC. Generally, when two metal elements form an intermetallic compound the unlike-atom distance is often smaller than half of the sum of the two like-atom distances, but does not equal any of them. Our results on the atomic distances resemble those of XAFS in both r_{CuCu} and r_{CuSn}. The r_{CuSn} by AIMD simulation is about 6.3% shorter than the arithmetic mean of the r_{CuCu} and r_{SnSn}. This also implies that Cu–Sn bonding exists in liquid Cu_6Sn_5 alloy, but its strength would not be as strong as that revealed by RMC.

Secondly, we pay attention to the profiles of these curves. For $g_{CuCu}(r)$ and $g_{CuSn}(r)$ the four curves fit each other rather well beyond the first minimum. In the region of the first peak, the curve by RMC has the smallest r_{CuSn} and the largest r_{CuCu} among the four curves [4], while AIMD simulation results in reasonable r_{CuCu} and r_{CuSn} compared with those from experiments. The largest heights in both $g_{CuCu}(r)$ and $g_{CuSn}(r)$ are given by RMC and AIMD simulation, respectively.

However, there is an apparent discrepancy in the profile of $g_{SnSn}(r)$ between calculated and experimental results. For $g_{SnSn}(r)$, RMC gives the same first peak position as XAFS [3]. The curve by North *et al* [2] has a little larger first peak position but nearly the same height as XAFS. AIMD simulation has a first peak position near that by North *et al*, but has the most diffused and asymmetric first peak.

At 0.628 nm in $g_{SnSn}(r)$ by Noth *et al* the second peak was located. XAFS did not extend the curves beyond about 0.38 nm. AIMD simulation reveals a second peak at about 0.66 nm, associated with a subpeak at about 0.52 nm which has not been discovered by other methods.

In order to verify whether the subpeak is a structural characteristic or an artificial peak, we performed other simulations for *l*-Cu_6Sn_5 alloy at 2073 K with the same density as at 913 K, and for *l*-$Cu_{85}Sn_{15}$ (at 1223 K) and *l*-$Cu_{15}Sn_{85}$ (at 803 K) alloys. The $g_{SnSn}(r)$'s are then plotted in figure 4 together with that of *l*-Cu_6Sn_5 alloy at 913 K. We find that, at much higher temperatures, the position of the subpeak is hardly changed, but its height is enhanced relatively. The subpeak is even more pronounced in *l*-$Cu_{85}Sn_{15}$ alloy, but hardly perceived in *l*-$Cu_{15}Sn_{85}$ alloy. This implies that the subpeak between the first and second peaks in $g_{SnSn}(r)$ is indeed a structural feature of *l*-Cu_6Sn_5 alloy. Here we provide only a straightforward explanation for this phenomenon. Detailed surveys on the composition dependence of the structure of liquid Cu–Sn alloys are to be carried out soon. Since the partial coordination numbers N_{SnSn} are found to decrease as the content of Sn decreases, while they decrease with increasing temperature, we think that in *l*-Cu–Sn alloys when the N_{SnSn}

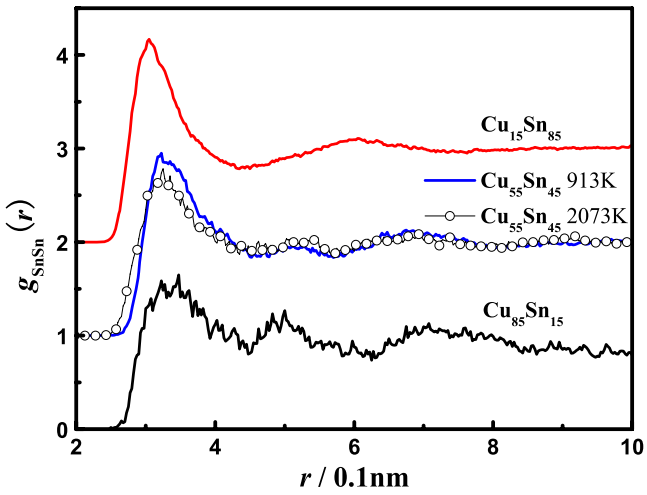

Figure 4. Comparison of PCFs of l-Cu_6Sn_5 alloy at different temperatures with that of l-$Cu_{15}Sn_{85}$ and l-$Cu_{85}Sn_{15}$ alloys.

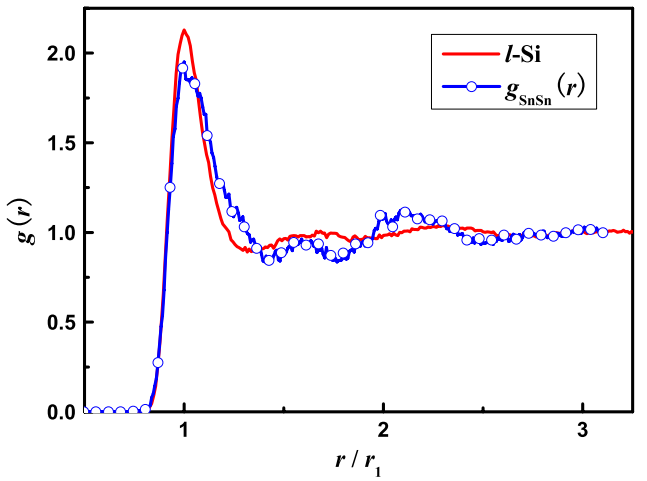

Figure 5. Comparison between PCF of l-Si and $g_{SnSn}(r)$ of l-Cu_6Sn_5 alloy.

is smaller, the covalent nature of Sn–Sn correlation becomes more important.

We have also tested whether the energy cutoff of the plane wavefunction sets and the spin of the electrons would influence the subpeak. If the energy cutoff is changed to 1.2 times 273 eV, no obvious difference is observed in the structural patterns. Also little difference has been made to the subpeak and the whole profile of the partial PCFs by considering the spin of the electrons.

Up to now, there are some research works on the structure of liquid Si [14–16] and liquid Sn [17, 18]. In general it is thought that covalent bonds partially exist in both l-Si and l-Sn, and that β-Sn local structure is employed to model both l-Si and l-Sn. To get more insight into the partial structure of Sn atoms in liquid Cu_6Sn_5 alloy, it is useful to compare $g_{SnSn}(r)$ with $g(r)$ of l-Si [14] as shown in figure 5, in which each PCF is rescaled on its horizontal axis by its first peak position (termed r_1 in figure 5).

We find that both the $g_{SnSn}(r)$ and l-Si curves have a subpeak at nearly the same position $r/r_1 = 1.60$.

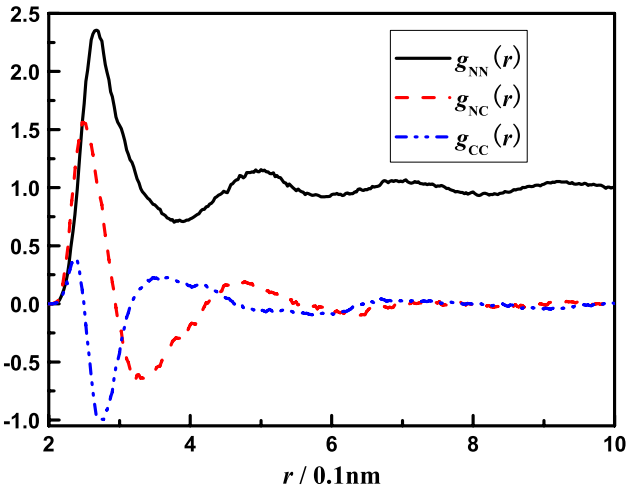

Figure 6. The BT partial correlation functions of l-Cu_6Sn_5 alloy.

Table 2. Partial coordination numbers of liquid Cu_6Sn_5 alloy.

α	β	r_{min} (nm)	$N_{\alpha\beta}$	$R_{\alpha\beta}$ (%)	Nominal (%)
Cu	Cu	0.349	4.74	47.6	54.55
Cu	Sn	0.377	5.23	52.4	45.45
Sn	Cu	0.377	6.27	41.7	54.55
Sn	Sn	0.460	8.76	58.3	45.45

According to [15], among several structural models, only the topologically disordered β-Sn-type structure can produce this subpeak for liquid Si. In crystalline β-Sn structure [19], there are coordination shells around $r/r_1 = 1.56$, while in diamond-type silicon the second shell is located at $r/r_1 = 1.63$. However, in a diamond-type structure the coordination number in the first shell should be near 4. Then the subpeak in $g_{SnSn}(r)$ of l-Cu_6Sn_5 alloy can be regarded as the same structural characteristic which was modeled by the topologically disordered β-Sn-type structural units in l-Si.

Thirdly, we will supply some chemical information on l-Cu_6Sn_5 alloy. According to [4] the l-Cu_6Sn_5 alloy has a self-coordination trend. We tried to examine this topic by employing the BT partial correlation functions. Here $g_{NN}(r)$ describes the sites of the scattering nuclei but does not distinguish between the chemical species that occupy those sites, $g_{CC}(r)$ describes the chemical ordering and has positive or negative peaks when there is a preference for like or unlike neighbors, respectively, and $g_{NC}(r)$ describes the correlation between sites and their occupancy by a given chemical species.

The BT PCFs of l-Cu_6Sn_5 alloy are shown in figure 6. $g_{NN}(r)$ shows rather strong topological short-range order with an asymmetric first peak which results from different atomic radii of both Sn and Cu. It is interesting to note that $g_{CC}(r)$ has a negative peak, which implies the chemical short-range order between unlike atoms.

We further analyze the constitutional proportion of the three elements in the partial coordination numbers. Here we define $R_{\alpha\beta}$ as the ratio of the proportion of the population of element β in the partial coordination number of element α and $R_{\alpha\beta} = N_{\alpha\beta}/(N_{\alpha\alpha} + N_{\alpha\beta})$. Such values are compiled in table 2.

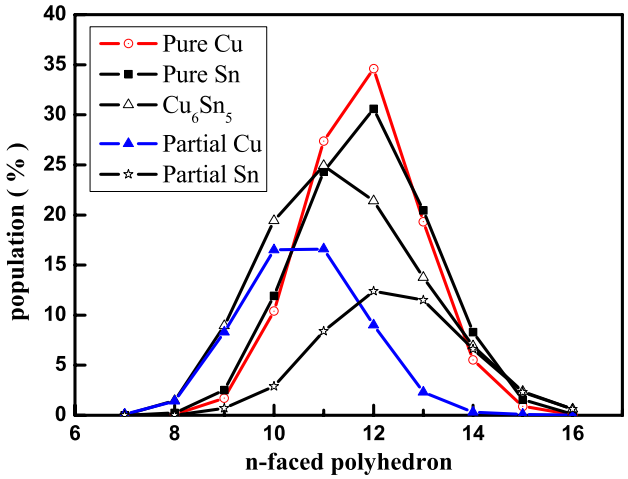

Figure 7. The population of n-faced polyhedra in l-Sn, l-Cu and l-Cu_6Sn_5 alloy.

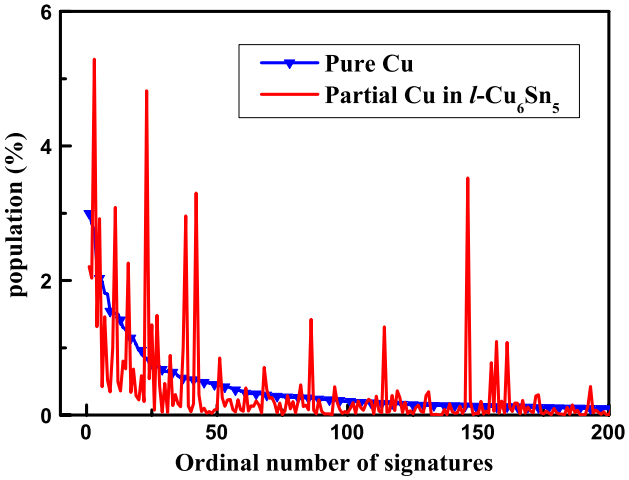

Figure 8. Comparison of the partial population of the signatures of Cu in l-Cu_6Sn_5 alloy with that of l-Cu.

In table 2 amongst the nearest neighbors of Sn, the constitutional proportion of Sn atoms is 58.3%, which is markedly higher than its nominal values. This suggests that Sn tends to attract more Sn atoms than a random distribution. Around a Cu atom, the constitutional proportion of Cu atoms is 47.6%, which is markedly less than its nominal values, which suggest that there may be less Cu–Cu bonding. But for unlike atoms the trends are in conflict with each other from both Sn and Cu sides. Cu tends to have more Sn atoms but Sn tends to have less Cu atoms. This situation is unusual in liquid alloys to our knowledge.

We have also calculate the Cargill–Spaepen chemical short-range order [20] by equation $\eta_{\mathrm{CuSn}} = Z_{\mathrm{CuSn}}/Z^*_{\mathrm{CuSn}} - 1$, in which $Z^*_{\mathrm{CuSn}} = c_{\mathrm{Sn}}Z_{\mathrm{Cu}}Z_{\mathrm{Sn}}/(c_{\mathrm{Cu}}Z_{\mathrm{Cu}} + c_{\mathrm{Sn}}Z_{\mathrm{Sn}})$. In this way, we get $\eta_{\mathrm{CuSn}} = -0.055$, which means that there is a weak tendency for compound formation. This is consistent with that drawn by BT correlation functions.

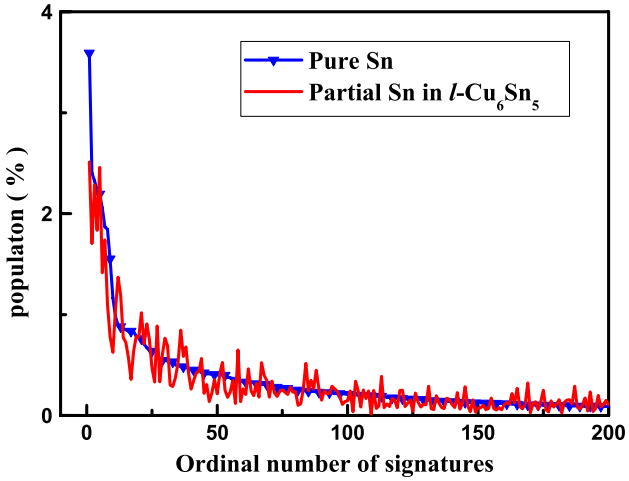

Figure 9. Comparison of the partial population of the signatures of Sn in l-Cu_6Sn_5 alloy with that of l-Sn.

4. Voronoi analysis

To make clear the local environment of both Sn and Cu atoms in liquid Cu_6Sn_5 alloy, we performed Voronoi analysis [21, 22] on the configurations from AIMD simulation, and employed a signature to represent the shapes of the polyhedron: (n_3, n_4, n_5, n_6), i.e. n_j is the number of j-sided faces.

As shown in figure 7, pure Cu and pure Sn have similar distribution via the n-faced polyhedrons, where n is the sum of n_j in the signature (n_3, n_4, n_5, n_6). However, in liquid Cu_6Sn_5 alloy, the distribution of the partial population of Sn and Cu atoms differs markedly from that of pure liquid Sn or liquid Cu. Partial Sn has the same maximum at 12 though the curve of partial Sn is much lower than that of pure Sn. Partial Cu has a very different curve from pure Cu. This means that, after alloying, the population of the n-faced polyhedrons around a Cu atom is very different from that in pure Cu, while an Sn atom has a similar distribution with that in pure Sn.

To make the difference clearer, we take signatures of pure Cu as the reference system to make a comparison with that of partial Cu in l-Cu_6Sn_5 alloy. First we sort the signatures by populations in descending order, and then pick the same signatures in the partial Cu signature set. The comparison is plotted in figure 8. It is found that the difference of the signature distribution is markedly different.

Then we take the pure Sn signature set as the reference, the population of the signature of partial Sn in l-Cu_6Sn_5 alloy is investigated, and the result is plotted in figure 9. It is found that the population of the signature vibrates along that of l-Sn slightly. They exhibit rather similar behavior.

By Voronoi analysis, it is found that the local structure of partial Sn in l-Cu_6Sn_5 alloy resembles that of l-Sn, while the local environment of Cu atoms in l-Cu_6Sn_5 alloy is largely different from that in l-Cu.

5. Electronic structure

In order to understand the bonding character in l-Cu_6Sn_5 alloy, its local densities of states (LDOSs) have been calculated.

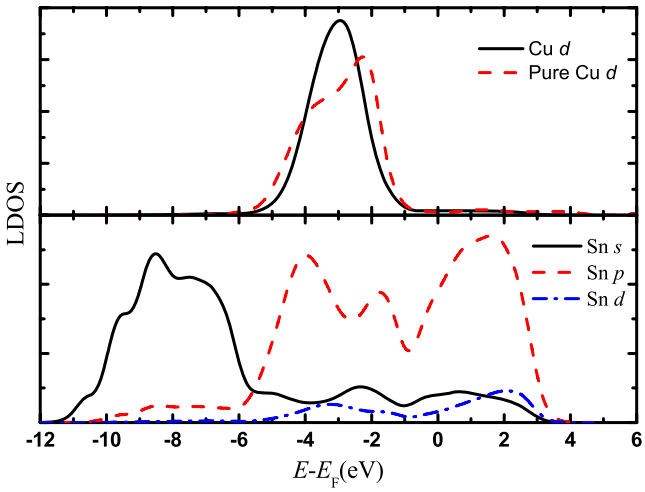

Figure 10. Local density of states of both Cu and Sn atoms in liquid Cu_6Sn_5 alloy.

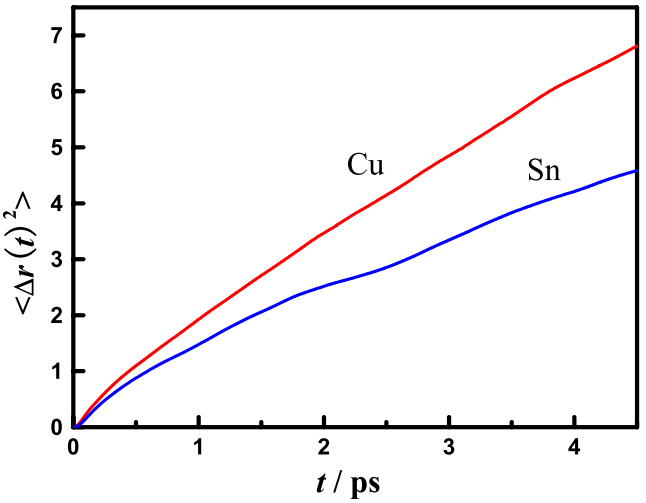

Figure 11. The time dependence of the MSD of atoms in l-Cu_6Sn_5 alloy.

In figure 10 only parts of the PDOS of both Cu and Sn atoms in liquid pure elements and liquid alloy were plotted. We neglect the other PDOS since either they are very small or they have plain changes compared with those in the liquid pure elements. We observe that at about −1.7 eV the characteristic of the s–p hybridization of Sn atoms in l-Sn is still visible in l-Cu_6Sn_5 alloy, while such a characteristic at about −6.6 eV is invisible in the liquid alloy. For s electrons of Sn atoms the peak at −8.5 eV is enhanced, perhaps due to their interaction with the s electrons of Cu. After alloying with Cu, a significant change takes place in the PDOS of p electrons of Sn atoms. A single peak at −1.5 eV has been split into double peaks at −1.7 and −4.0 eV where the main peak is located. This is correlated with the marked change in the PDOS of d electrons of Cu atoms in l-Cu_6Sn_5 alloy and manifests the hybridization between p electrons of Sn atoms and d electrons of Cu atoms.

Overall Cu–Sn and Sn–Sn bonding is found in l-Cu_6Sn_5 alloy. We think that the electron density distribution of the Sn atoms is markedly modified by alloying with the Cu atoms; then the Sn–Sn bonding nature changes from more metallic in l-Sn to more covalent in l-Cu_6Sn_5 alloy.

6. Dynamical properties

Firstly, we studied the diffusion of atoms in the liquid by calculating the time-dependent mean-square displacement (MSD) defined in the usual way for species α as

$$\langle \Delta r(t)^2 \rangle = \frac{1}{N_\alpha} \left\langle \sum_{i=1}^{N_\alpha} |r_{\alpha i}(t+t_0) - r_{\alpha i}(t_0)|^2 \right\rangle, \tag{8}$$

where the sum goes over all N_α atoms of species α, t_0 is an arbitrary time origin and the angle brackets denote a thermal average or equivalently an average over time origins. The MSD over time is plotted in figure 11.

For diffusing liquids the MSD is linear in t for large time, and the slope is proportional to the diffusion coefficient D_α of species α:

$$\langle \Delta r(t)^2 \rangle \to 6D_\alpha t + B_\alpha, \tag{9}$$

where B_α is constant. The unit of the diffusion coefficient in this paper is 10^{-5} cm^2 s^{-1}. For Cu atoms the present work gives 2.45; unfortunately, we cannot find the corresponding experimental value for l-Cu_6Sn_5 alloy. For Sn atoms D_{Sn} is 1.60 (913 K), which is much less than its experimental value of 7.5 (1073 K) [23].

To verify the calculated results, we evaluate the viscosity of l-Cu_6Sn_5 alloy by using the relationship with the diffusion coefficient through the Stokes–Einstein equation:

$$\eta = \frac{k_B T}{2\pi a D}, \tag{10}$$

where $D = (D_{Cu} + D_{Sn})/2$ and a is the effective 'diameter' of the diffusing particles. We define the particle size a as the average value of the nearest-neighbor distances of Cu–Cu, Cu–Sn and Sn–Sn from table 1 which results in 0.283 nm. The calculated viscosity of l-Cu_6Sn_5 alloy is 3.4 mPa s, which is in good agreement with its experimental value ∼3.25 mPa s [24].

We also evaluate the diffusion coefficients for both l-Sn and l-Cu and compared them with those from the literature. The present work gives D_{Sn} and D_{Cu} as 4.1 (873 K) and 3.6 (1473 K), respectively, for l-Sn and l-Cu. The available D_{Sn}'s for l-Sn are 5.5 (825 K) [25], 3.0 (573 K) [17] and 3.6 (873 K) [18]. D_{Cu} is found to be 3.97 for l-Cu [26]. By comparison we think that our results on D_{Sn} and D_{Cu} for l-Sn and l-Cu are reasonable.

More detailed information about the single-particle dynamics can be obtained by studying the velocity autocorrelation function defined as

$$\psi(t) = \frac{\langle V_i(0) \cdot V_i(t) \rangle}{\langle V_i(0) \cdot V_i(0) \rangle}, \tag{11}$$

where $V_i(t)$ is the velocity of particle i and the brackets $\langle\,\rangle$ denote an average over particles and over time origins. The corresponding spectral density $Z(\nu)$ is given by

$$Z(\nu) = \int_0^\infty \psi(t) \cos(2\pi\nu t)\, \mathrm{d}t. \tag{12}$$

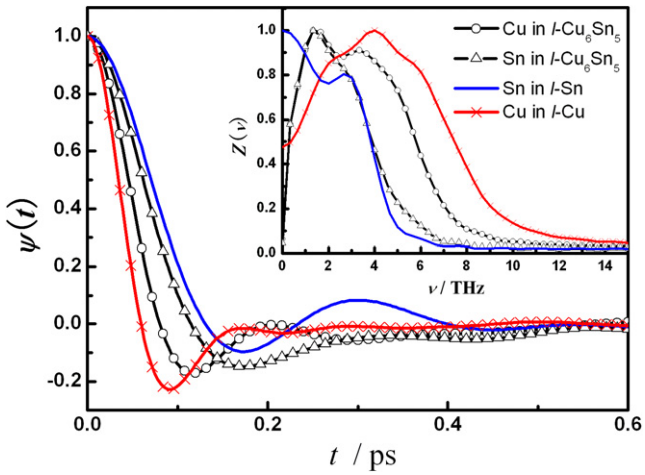

Figure 12. Velocity autocorrelation functions and the corresponding spectral densities (inset) of l-Cu_6Sn_5 alloy and l-Sn and l-Cu.

From figure 12 we find that all four curves for $\psi(t)$ have negative minima which are often regarded as the behavior of simple liquids [17]. However, the depth is different in the way that l-Cu has the deepest minimum, while the l-Sn is the shallowest. l-Sn has a peak at 2.8 THz, while Sn atoms in l-Cu_6Sn_5 alloy have a shoulder at about 3.0 THz. The covalent Sn dimer has an experimental vibrational frequency of about 5.7 THz [27], which is close to the peak around 3.0 THz. The fact that the spectrum of Cu atoms in l-Cu_6Sn_5 alloy shifts towards the left from l-Cu implies that Cu atoms in l-Cu_6Sn_5 alloy have a less close-packed environment than atoms in l-Cu.

7. Summary

In summary, the complex structure of liquid Cu_6Sn_5 alloy is revealed by the AIMD simulations. The hetero-coordination tendency is manifested by BT pair correlation functions and the chemical short-range order parameter. On the other hand, the preference for self-coordination of Sn atoms is suggested by Voronoi analysis and the partial coordination number analysis. Moreover, the $g_{SnSn}(r)$ by AIMD simulation is distinguished from those by experiments and RMC methods through a subpeak located in between the conventional first and second peaks. A fraction of the topologically disordered β-Sn-type structural units are suggested to survive in liquid Cu_6Sn_5 alloy. The LDOS analysis provides that Cu–Sn and Sn–Sn bonding exists in the liquid Cu_6Sn_5 alloy.

Finally, we have to say that we are in a quandary. On the one hand, the experimental techniques employed so far in the investigation of liquid Cu_6Sn_5 alloy seem overwhelming. On the other hand, the AIMD simulation is thought to be a very successful tool in the study of liquid alloys. However, the discrepancy between the $g_{SnSn}(r)$ by AIMD simulation and that by experiments could not be thought to be negligible. We then suggest that both the experimental and theoretical results should be counterchecked by other methods.

Acknowledgments

This work was supported by the National Natural Science Foundation of China (grant nos. 50571053, 50631010) and the National Basic Research Program 973 (2007CB613901). We also thank the Shandong High Performance Computing Center for providing computational time.

References

[1] Enderby J E, North D M and Egelstaff P A 1966 *Phil. Mag.* **14** 961
[2] North D M and Wagner C N J 1970 *Phys. Chem. Liq.* **2** 87
[3] Trapananti A and Di Cicco A 2004 *Phys. Rev.* B **70** 014101
[4] Kaban S G, Hoyer W, Jóvári P, Delaplane R G and Wannberg A 2005 *Phys. Chem. Glasses* **46** 472
[5] Larsson A K, Stenberg L and Lidin S 1994 *Acta Crystallogr.* B **50** 636
[6] Jakse N, Le Bacq O and Pasturel A 2004 *Phys. Rev. Lett.* **93** 207801
[7] Kresse G and Furthmuller J 1996 *Comput. Mater. Sci.* **6** 15
[8] Kresse G and Joubert D 1999 *Phys. Rev.* B **59** 1758
[9] Perdew J P and Wang Y 1992 *Phys. Rev.* B **46** 6671
[10] Nosé S 1984 *J. Chem. Phys.* **81** 511
[11] Fischer H E, Barnes A C and Salmon P S 2006 *Rep. Prog. Phys.* **69** 233
[12] Waseda Y 1980 *The Structure of Non-Crystalline Materials* (New York: McGraw-Hill) p 278
[13] Qin J Y, Wang W M, Bian X F and Sliusarenko S I 1998 *Acta Phys. Sin.* **47** 438
[14] Gu T K, Qin J Y, Xu C Y and Bian X F 2004 *Phys. Rev.* B **70** 144204
[15] Ogawa H and Waseda Y 1994 *Z. Naturf.* A **49** 987
[16] Štich I, Car R and Parrinello M 1989 *Phys. Rev. Lett.* **63** 2240
[17] Calderín L, González D J, González L E and López J M 2008 *J. Chem. Phys.* **129** 194506
[18] Itami T *et al* 2003 *Phys. Rev.* B **67** 064201
[19] Wolcyrz M, Kubiak R and Maciejewski S 1981 *Phys. Status Solidi* b **107** 245
[20] Cargill G S III and Spaepen F 1981 *J. Non-Cryst. Solids* **43** 91
[21] Watanabe M S and Tsumuraya K 1987 *J. Chem. Phys.* **87** 4891
[22] Medvedev N N 1986 *J. Comput. Phys.* **67** 223
[23] Grinevich G P, Kapitanchuk L M and Polishchuk T V 1978 *Russ. Phys. J.* **21** 1369
[24] Mao T *et al* 2007 *Physica* B **387** 1
[25] Bruson A and Gerl M 1980 *Phys. Rev.* B **21** 5447–54
[26] Iida T and Guthrie R I L 1988 *The Physical Properties of Liquid Metals* (Oxford: Clarendon)
[27] Bondybey V E, Heaven M and Miller T A 1983 *J. Chem. Phys.* **78** 3593